AFRL-ML-WP-TP-2007-496

UNIQUE FEMTOSECOND MICROMACHINING METHODS IN SEMI-INSULATING AND CONDUCTING SILICON CARBIDE (PREPRINT)

Chris Brewer, Don Dorsey, Angela Campbell, and Shane Juhl

Materials and Manufacturing Directorate

APRIL 2007

AIR FORCE RESEARCH LABORATORY
MATERIALS AND MANUFACTURING DIRECTORATE
WRIGHT-PATTERSON AIR FORCE BASE, OH 45433-7750
AIR FORCE MATERIEL COMMAND
UNITED STATES AIR FORCE

NOTICE AND SIGNATURE PAGE

Using Government drawings, specifications, or other data included in this document for any purpose other than Government procurement does not in any way obligate the U.S. Government. The fact that the Government formulated or supplied the drawings, specifications, or other data does not license the holder or any other person or corporation; or convey any rights or permission to manufacture, use, or sell any patented invention that may relate to them.

This report was cleared for public release by the Air Force Research Laboratory Wright Site (AFRL/WS) Public Affairs Office and is available to the general public, including foreign nationals. Copies may be obtained from the Defense Technical Information Center (DTIC) (http://www.dtic.mil).

AFRL-ML-WP-TP-2007-496 HAS BEEN REVIEWED AND IS APPROVED FOR PUBLICATION IN ACCORDANCE WITH ASSIGNED DISTRIBUTION STATEMENT.

*//Signature//

CHRISTOPHER D. BREWER, Ph.D.
Direction Mgr, Space Systems Hardening
Exploratory Development
Hardened Materials Branch

//Signature//

MARK S. FORTE, Acting Chief
Hardened Materials Branch
Survivability and Sensor Materials Division

//Signature//

TIM J. SCHUMACHER, Chief
Survivability and Sensor Materials Division

This report is published in the interest of scientific and technical information exchange, and its publication does not constitute the Government's approval or disapproval of its ideas or findings.

*Disseminated copies will show "//Signature//" stamped or typed above the signature blocks.

REPORT DOCUMENTATION PAGE

Form Approved
OMB No. 0704-0188

1. REPORT DATE *(DD-MM-YY)*	2. REPORT TYPE	3. DATES COVERED *(From - To)*
April 2007	Journal Article Preprint	

4. TITLE AND SUBTITLE

UNIQUE FEMTOSECOND MICROMACHINING METHODS IN SEMI-INSULATING AND CONDUCTING SILICON CARBIDE (PREPRINT)

5a. CONTRACT NUMBER
In-house

5b. GRANT NUMBER

5c. PROGRAM ELEMENT NUMBER
62102F

6. AUTHOR(S)

G. Logan DesAutels, Marc Finet, Scott Ristich, and Matt Whitaker (AT&T Government Solutions)
Chris Brewer, Don Dorsey, Angela Campbell, and Shane Juhl (AFRL/ML)
Peter Powers, Qiwen Zhan, and Weibin Chen (University of Dayton)
Mark Walker (General Dynamics Information Technology, Inc.)

5d. PROJECT NUMBER
4348

5e. TASK NUMBER
RG

5f. WORK UNIT NUMBER
M08R1000

7. PERFORMING ORGANIZATION NAME(S) AND ADDRESS(ES)

AT&T Government Solutions
Dayton, OH 45433

University of Dayton
Dayton, OH 45469

Materials and Manufacturing Directorate (AFRL/ML)
Wright-Patterson Air Force Base, OH 45433-7750
Air Force Materiel Command
United States Air Force

General Dynamics Information Technology, Inc.
5100 Springfield Pike, Suite 509
Dayton, OH 45431-1264

8. PERFORMING ORGANIZATION REPORT NUMBER
AFRL-ML-WP-TP-2007-496

9. SPONSORING/MONITORING AGENCY NAME(S) AND ADDRESS(ES)

Air Force Research Laboratory
Materials and Manufacturing Directorate
Wright-Patterson Air Force Base, OH 45433-7750
Air Force Materiel Command
United States Air Force

10. SPONSORING/MONITORING AGENCY ACRONYM(S)
AFRL/MLPJA

11. SPONSORING/MONITORING AGENCY REPORT NUMBER(S)
AFRL-ML-WP-TP-2007-496

12. DISTRIBUTION/AVAILABILITY STATEMENT
Approved for public release; distribution unlimited.

13. SUPPLEMENTARY NOTES
Journal article submitted to Journal of Optics A; Pure and Applied Optics. The U.S. Government is joint author of this work and has the right to use, modify, reproduce, release, perform, display, or disclose the work. PAO Case Number: AFRL/WS 07-0774, 03 Apr 2007.

14. ABSTRACT

Femtosecond laser pulses were used to write volume phase gratings in bulk 6H semi-insulating and conducting Silicon Carbide (SiC); a wide bandgap semiconductor material provided by Wright-Patterson AFB AFRL/MLPS. Gratings were micro-machined into these materials using a novel anamorphic lens design and an automated x, y, z linear stage to control the sample position. The anamorphic lens reduced the circular laser beam distribution to a 2.5 μm gratings were manufactured for various laser energies, number of laser pulses, and grating line spacing using a direct write process. Single and multi-pulse femtosecond radiations are shown to lead to permanent index of refraction changes from the surface to approximately 10 μm below the surface of these bulk materials. Each grating was analyzed visually using a visible microscope and analytically by measuring the diffraction efficiency to determine the most efficient grating. Raman spectroscopy, atomic force microscopy (AFM), and near field scanning optical microscopy (NSOM) results are also presented.

15. SUBJECT TERMS
Atomic Force Microscopy (AFM), Near field Scanning Optical Microscopy (NSOM), Femtosecond Micromachining

16. SECURITY CLASSIFICATION OF:			17. LIMITATION OF ABSTRACT:	18. NUMBER OF PAGES	19a. NAME OF RESPONSIBLE PERSON (Monitor)
a. REPORT	b. ABSTRACT	c. THIS PAGE			Christopher D. Brewer
Unclassified	Unclassified	Unclassified	SAR	16	19b. TELEPHONE NUMBER *(Include Area Code)* N/A

Standard Form 298 (Rev. 8-98)
Prescribed by ANSI Std. Z39-18

Unique Femtosecond Micromachining Methods in Semi-insulating and Conducting Silicon Carbide

G. Logan DesAutels[1], Chris Brewer[2], Peter Powers[3], Mark Walker[4], Don Dorsey[5], Angela Campbell[5], Shane Juhl[6], Marc Finet[1], Scott Ristich[1], Matt Whitaker[1], Qiwen Zhan[3], Weibin Chen[3],

[1]AT&T Government Solutions, Dayton, OH 45433
[2]Air Force Research Laboratory, Materials and Manufacturing Directorate, MLPJE, WPAFB, OH 45433
[3]University of Dayton, Dayton, OH 45469
[4]General Dynamics Information Tech., Dayton, OH 45431
[5]Air Force Research Laboratory, Materials and Manufacturing Directorate, MLPSM, WPAFB, OH 45433
[6]Air Force Research Laboratory, Materials and Manufacturing Directorate, MLBP, WPAFB, OH 45433

Abstract – Femtosecond laser pulses were used to write volume phase gratings in bulk 6H semi-insulating and conducting Silicon Carbide (SiC); a wide bandgap semiconductor material provided by Wright-Patterson AFB AFRL/MLPS[1]. Gratings were micro-machined into these materials using a novel anamorphic lens design and an automated x, y, z linear stage to control the sample position. The anamorphic lens reduced the circular laser beam distribution to a 2.5μm by 190μm line or elliptical shape. Using this process a series of approximately 500μm x 500μm gratings were manufactured for various laser energies, number of laser pulses, and grating line spacing using a direct write process. Single and multi-pulse femtosecond radiations are shown to lead to permanent index of refraction changes from the surface to approximately 10μm below the surface of these bulk materials. Each grating was analyzed visually using a visible microscope and analytically by measuring the diffraction efficiency to determine the most efficient grating. Raman spectroscopy, atomic force microscopy (AFM), and near field scanning optical microscopy (NSOM) results are also presented.

TABLE OF CONTENTS

1. INTRODUCTION

Femtosecond (fs) lasers have become a very important tool for micromachining and fabrication of photonic devices. Their unique ability of inducing permanent index changes into just about any transparent material is due to fast focusing conditions, resulting in very high intensity causing nonlinear multi-photon absorption. Former research has theorized that the ultra-fast pulse is too short to interact at the molecular level, and instead interacts at the atomic electronic level[2,3]. Here the fs pulse displaces electrons permanently and/or causes lattice changes resulting in a modification to the index of refraction[2,3]. The modification to the index is localized to a very small volume depending on the NA and energy used. These index alterations can be on the surface or in most cases subsurface in bulk material.

SiC is an attractive alternative material for a variety of semiconductor devices where silicon (Si) lacks the hardness that carbon furnishes. These areas where SiC devices can be used include high-power high-voltage switching applications, high temperature electronics, and avionics where the reduction of payload due to many wires are needed to keep sensitive Si-based electronics away form extreme environments onboard aircrafts[4]. However, SiC has issues related to micro-machining due to its hardness.

SiC is also resistant to wet chemical etching and alternative methods to bulk micromachining this material include deep reactive ion etching (DRIE) and the most direct means to micromachining SiC is reactive ion etching (RIE)[5]. These methods of processing SiC have issues related to masking or micro-masking for etching purposes, low etching rates, and an increase of processing steps[5]. The method presented in this paper give alternate means of micro-machining SiC.

In this paper we discuss a new method of writing gratings in bulk transparent SiC materials using ultrafast laser pulses

(single and multi-pulses). We will also investigate the changes induced using a variety of techniques like Raman spectroscopy, atomic force microscopy (AFM), and near field scanning optical microscopy (NSOM) experiments.

Our method of micromachining gratings uses an anamorphic lens to distribute the ultrafast (UF) laser pulse from a 5.5mm round Gaussian distribution to a 2.5μm by 190μm line shape. The grating was micro-machined in soda lime glass (SLG) and SiC using automated xyz stages controlled by Labview in a direct write configuration. A chopper wheel in conjunction with a high speed shutter allowed single or multiple laser pulses to hit the sample. The fs laser pulses were generated using a Clark-MXR CPA-2010 laser system, with a wavelength of 780nm, a pulse width of 150-200fs, M^2 = 1.55 and a maximum energy of 1mJ/pulse. Grating structures were written into the SLG and SiC by successively machining 2.5 μm by 190 μm lines end-to-end to form an individual machined line. This process was repeated such that each grating consisted of three columns of 150-180μm long by 2.5μm wide index modified lines and 25 rows of center to center grating line spacing of 20μm. The individual grating lines overlap approximately 5-10μm.

This method of micromachining gratings is an alternative to interference techniques and/or circular spot direct writing using high speed translation of the sample. It provides accurate micro-machined gratings in the absence of any self-focusing issues due to the elliptical beam volume. It also shows that an elliptical beam has a much higher damage threshold than that of symmetrically round beams due to the lack of self-focusing in the substrate[6]. In our experiments, the numerical aperture is very small, which also results in a higher damage threshold[7]. The idea is that a small NA in combination with an elliptical beam will decrease the chances of any self-focusing occurring within the bulk of the sample. Self-focusing will not only spoil the micro-machined features but the filamentation of the femtosecond beam will result in a very unpredictable/undesired micro-machined features. The gratings produced with the anamorphic lens resist any nonlinear self-focusing attributes, and results in "clean" accurate gratings.

2. Experimental Setup

In this section we discus the experimental setup for micromachining the gratings in transparent materials using femtosecond laser technology.

The experimental setup used in this study is shown in Figure 1.

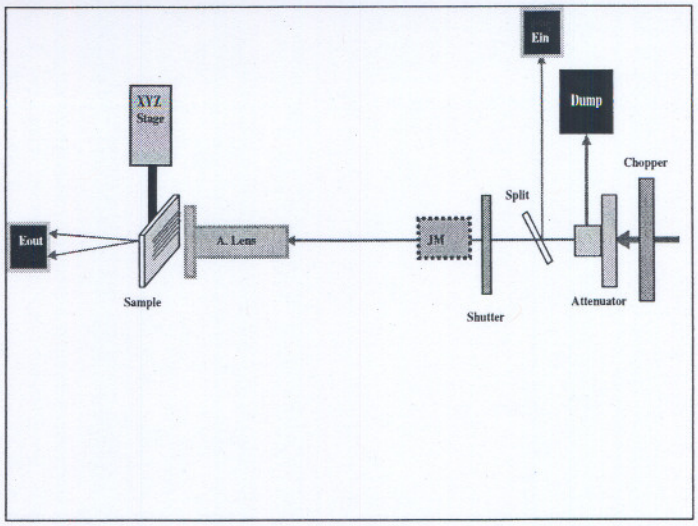

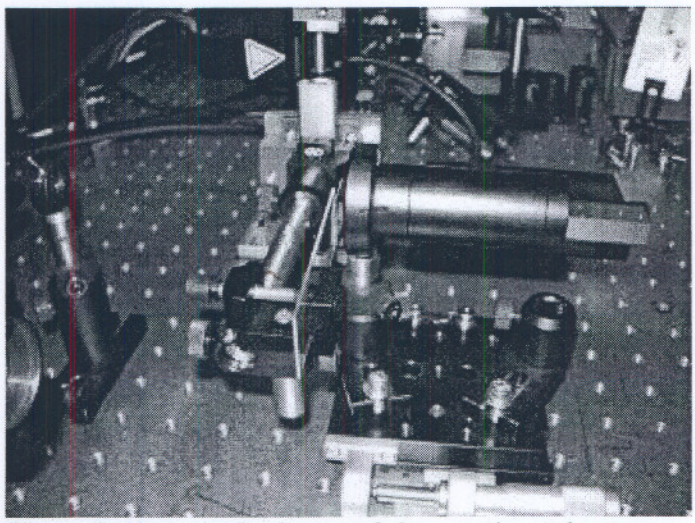

Figure 1 Above is the layout of the experimental setup, using the anamorphic lens. Below is a picture of the Anamorphic lens aligned to the SiC sample that is mounted on an xyz stage.

Here the Ein photodiode is used as a trigger for the high speed shutter and to measure the input beam, while the transmit diode, Eout, measures the transmission through the sample. If damage occurs then the transmission will drop accordingly. A joule meter, shown in the bottom picture of Figure 2, is used to calibrate the reference diode; records every single pulse that hits the sample. A Cohu CCD camera is used to profile and measure the M^2 of the beam before each experiment. Spiricon, Inc. software is used to profile and measure the M^2.

Labview was used to control the 3 axis stage, the λ/2-plate, the high speed shutter, and the Ein/Eout photodiodes. As the 500Hz laser pulses propagate to the chopper, all but two of the twenty-four spokes are masked off allowing pulses through. This drops the frequency to 41.667Hz for $1/12^{th}$ of the laser's 500Hz, while the high speed shutter can further select just a single pulse. The λ/2-waveplate is mounted in a computer-controlled rotation stage in conjunction with a

polarizer so that the transmitted pulse energy is controlled by rotating the half-wave plate. The beam splitter shown in figure 1 cuts the beam down to ~ 4-5% of the pulse for the Ein photodiode and the rest passes through to the sample. The xyz-stage controller positions the sample to within ±3μm accuracy in each axis. A Joule meter is used to calibrate the Ein/Eout photodiodes, and is traceable to NIST standards. For each λ/2-plate angle, the energy is associated and a calibration of Eout versus Ein slope calculated. Each data run results in a calibration plot and a transmission verses input energy or fluence. This measurement allows for the characterization of the damage threshold. Transmission verses Fluence plots are shown later in Sections 4 and 5.

3. ANAMORPHIC LENS DESIGN

3.1. Zemax Design and Analysis

The design and analysis of this anamorphic lens design was accomplished using Zemax. Figure 2 below shows some different views of the anamorphic lens.

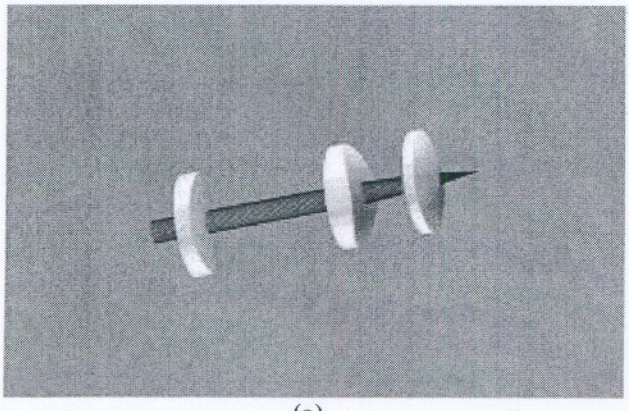

(a)

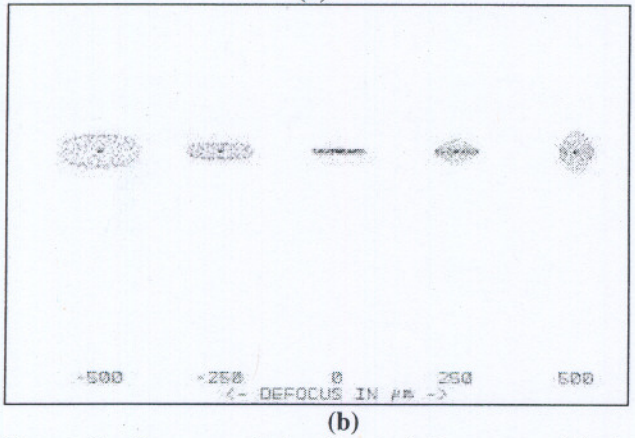

(b)

Figure 2 Zemax analytic views of the anamorphic lens used spread the focused beam elliptically. (a) is a Zemax solid layout displaying each lens and their relative position in the lens tube (on the left is a 100mm focal in x, middle is a 50mm in y, and on the right is the spherical lens) , and (b) is a plot of the ray distribution through focus ± 200μm.

This lens shown in Figure 2 was designed to transform the 5.5mm circular beam into a 190μm by 2.5μm line distribution as shown in Figure 2 (b). The x-dimension uses a 100mm focal length lens and the y-dimension uses a 50mm focal length lens. The last lens is a spherical lens, which is used to further assist the x and y foci. The goal here was to redistribute the round Gaussian beam into a line spread. A spherical lens was used to assist the two cylindrical lenses to provide a line spread of high enough fluence above the damage threshold (DT) of SiC. This distribution serves multiple reasons in the micromachining process. First, the line distribution is used to quickly create gratings that are then used to measure the diffraction efficiency and ultimately change in magnitude of the processed area index of refraction. Second, the extremely fast focus limits the damage area to a line when the energy is low. Third, an elliptical beam prevents self-focusing effects that could potentially cause an unpredictable lensing affects and change the desired line spread.

Table 1 gives both experimental and theoretical NA results of the anamorphic lens. The geometrical NA values are in good agreement with the experimental values in x and y axes. Table 1 gives the results and compares those results with a commonly used spherical lens. The NA was determined for each axis by finding the slope of a series of points before/after the focus. The experimental and theoretical (using Zemax) data match within 10%.

Table 1: NA values for theoretical and experimental results.

Type	NAx	NAy
Theoretical	0.077	0.129
Experimental	0.077	0.116
Spherical 125mm Lens	0.021	0.021

4. DAMAGE THRESHOLD

Damage thresholds were measured prior to micromachining gratings in order to calculate the energy required to change the index of refraction of the desired bulk material. Damage threshold measurements were performed on three materials; fused silica (FS) was initially damaged tested to provide a baseline reference and for its abundance, semi-insulating SiC was the primary material of interest in this paper, and finally, conducting SiC for comparison of a conducting material with an insulating material.

The DT, measured in J/cm^2, is measured to determine what the beam distribution is needed to micro-machine gratings into the SiC material. Mathcad models calculate the spot size and fluence levels for the circular damage threshold and for the anamorphic beam spread threshold. The following equations are used for these calculations[8],

$$w_o = \frac{\lambda \cdot f \cdot M^2}{\pi \cdot w_z}, \qquad \text{Equation 1}$$

where f is the focal length, λ is the wavelength, w_z is the spot radius propagating from the laser and is also known as the clear aperture. The M^2 is a measured quantity and w_z is given below.

$$w_z = r \cdot \sqrt{1 + \left(\frac{Z}{Z_R}\right)^2}, \qquad \text{Equation 2}$$

where Z is the propagation distance from the laser source to the test bed, r is the beam radius measured at the laser source, and Z_R is the Rayleigh range. The peak fluence can be determined using

$$F_o = \frac{2 \cdot E}{\pi \cdot w_o^2}, \qquad \text{Equation 3}$$

where E is the input energy. The above equations were used for each axis for the elliptical beam formed by the anamorphic lens system. Table 2 gives the damage threshold results for FS, SiC SI, and conducting SiC.

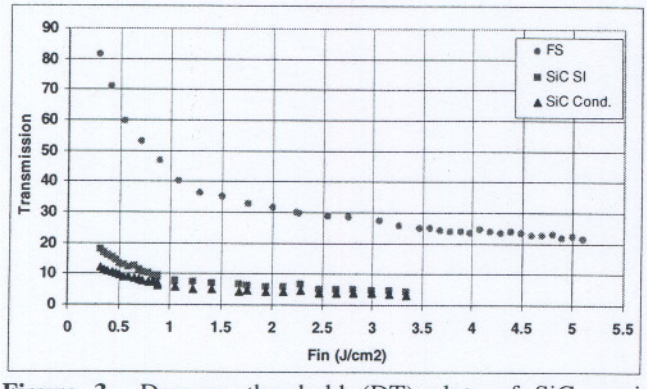

Figure 3 Damage threshold (DT) plots of SiC semi-insulating (SI), SiC conducting, and Fused Silica (FS). FS is our base-line sample, which is used to calibrate our DT experiments. FS has a DT that is well referenced to be around ~3.0-4.0 J/cm^2 as referenced[9].

These DT results greatly depend on NA as shown in Schaffer-Mazur[7]. In Figure 3, the FS data was recorded using a 125mm lens (NA = 0.022), while the SiC and FS samples DT were measured using a 175mm lens (NA = 0.016). For example, if NA of 0.016 was used to measure the FS, that threshold would tend to hold a lower value of fluence (DT<3.6 J/cm^2). Our facility will be investigating the NA dependence further in the near future, but for now these DT measurements are accurate enough to calculate the anamorphic beam distribution.

Table 2: DT measured results.

Sample	DT (J/cm^2)	Bandgap
FS	3.6	9eV[10]
SiC conducting	0.65	3.1eV[11,12]
SiC semi-insulating	0.6	3.1eV[11,12]

5. SiC Gratings

5.1. Grating Fabrication

Gratings were first fabricated in soda lime glass (SLG) to perfect our technique using the anamorphic lens for a single laser pulse. Each grating was then characterized using a visible microscope to visually inspect the gratings, and quantitatively by measuring the diffraction efficiency (DE). Figure 4 illustrates one of the SLG microscope images. This grating has a spacing of 20µm and consists of 25 rows (~450-500µm in the vertical) and 5 columns of ~90µm by ~10µm in the horizontal. The grating lines in Figure 4 are subsurface (~5-10µm), but the image was post processed to help visualize the grating lines for presentation purposes, thus causing them to appear to be above the surface.

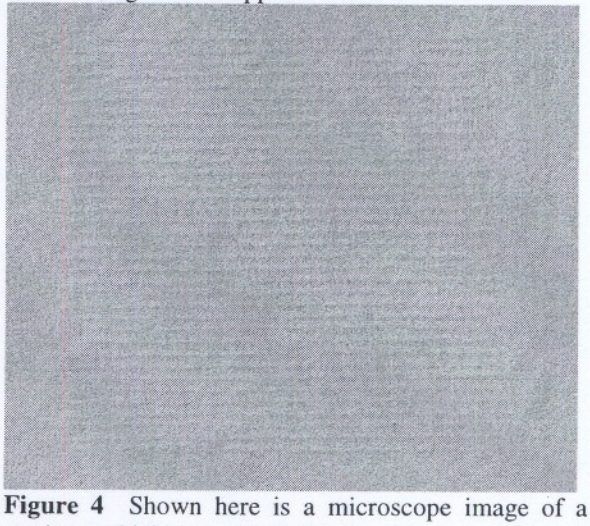

Figure 4 Shown here is a microscope image of a SLG grating, which has the following characteristics: fluence used was 2.8 J/cm^2 and measured a 1st order DE of 0.4% for a single pulse.

A typical DE measurement output is shown in Figure 5. This DE output shows the 0-order and diffracted beams resulting from a HeNe laser at 632.8nm, 1.5mm 1/e^2 beam diameter, and 1.5mW output power A long focal length lens was used to keep the depth of focus (or Rayleigh range) large and the spot size close to 500µm, which is roughly the size of the grating structures. The HeNe beam power and diameter were measured with Spiricon software and a Cohu CCD camera with and without the sample (in the absence of the gratings). The HeNe illuminated a specific grating in the sample and the zero-order (left picture in Figure 5) and 1st order (right picture in Figure 5 encompassed with a white circle) output beams were measure with Spiricon/Cohu. Images of the zero-order beam and 1st order diffraction pattern are shown in Figure 5.

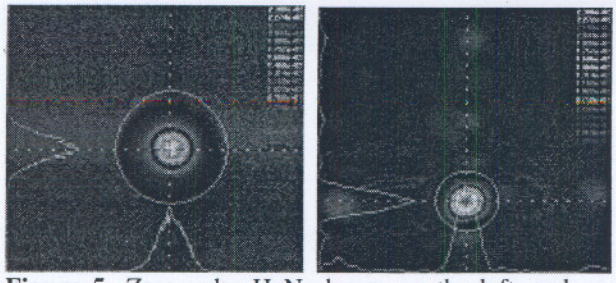

Figure 5 Zero-order HeNe beam, on the left, and on the right is the 1st order diffraction pattern resulting from one of the SLG gratings.

The DE of the 1st order diffraction pattern in Figure 5 was calculated by first measuring the power of the 1st order then using the following equation,

$$DE = \frac{2 \cdot P_1 \cdot 10^{-(ND_o - ND_1)}}{P_o} \cdot 100. \quad \text{Equation 4}$$

In Equation 4, P_1 is the 1st order measured power, P_o is the zero-order power, ND_o is the density filter OD placed in front of the Cohu camera when measuring the zero-order beam (no grating present only the unprocessed sample), and ND_1 is the neutral density filter OD placed in front of the Cohu camera while measuring the 1st order diffraction pattern.

The SLG grating with a spacing of 20μm has very low 1st order diffraction efficiency; maximum DE is only ~0.37%. Increasing the energy/fluence levels to increase the DE caused the surface of the grating substrate to begin to "char" (thermal breakdown of the molecular lattice due to the inability for the crystal to dissipate heat).

5.2. SiC Semi-insulating Grating Data/Results

Gratings were made in semi-insulating SiC using the anamorphic lens technique described earlier under the following conditions: single and multi laser pulses, varying energy levels, and varying grating spacing. Each grating was characterized using a visible microscope and quantitatively by measuring the diffraction efficiency (DE). Figure 6 shows a SiC grating with a spacing of 20μm, 25 rows, and 3 columns of ~170μm by ~2.5μm. These gratings have a volume of approximately 30-40μm deep; depending on the fluence level. That is, a surface grating will extend to ~30-40μm below the surface creating a volume grating. This is true for both SLG and SiC materials. The depth was determined using a visible microscope with a 50x objective. A 50x objective has a short depth of focus that gives a fairly good estimate of the depth of the grating structures.

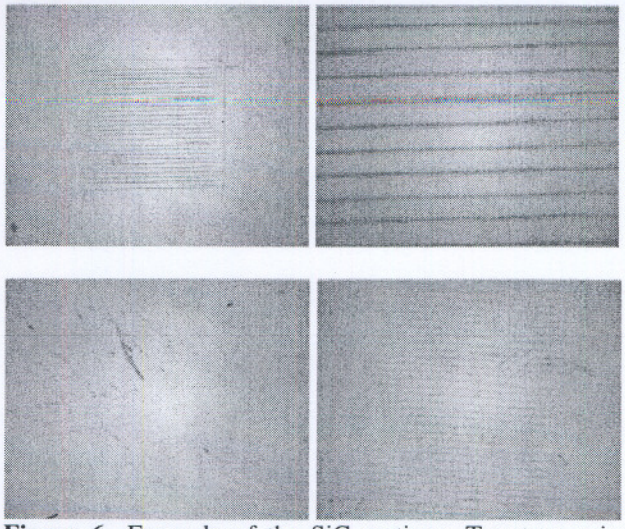

Figure 6 Example of the SiC gratings, Top two, micro-machined using 4μJ at 36 pulses, a grating separation of 20μm, and a line width of 2.5μm. The bottom two images represent a subsurface grating in SiC – on the bottom left is an image of the SiC surface, and on the bottom right is the subsurface grating approximately 30-40μm below the surface.

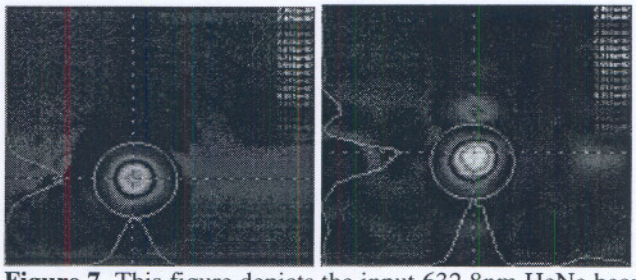

Figure 7 This figure depicts the input 632.8nm HeNe beam and the resulting SiC diffraction pattern of the first order.

Figure 7 gives the input HeNe 632.8nm beam and the output SiC diffraction pattern. The gratings have a slightly different geometry than the SLG gratings, but the general diffraction patterns are very similar. The SiC grating geometries are thinner, longer, and have a smaller overlap causing less visible higher order diffraction patterns.

Fabrication scenarios of the SiC gratings consisted of the following:

1. Variable energy.
2. Variable pulses for each energy tested.
3. Variable grating spacing at constant energy and number of pulses.
4. Semi-insulating verses conducting samples.

Each of the above were evaluated by charting the DE verses energy, number of pulses and grating spacing. In Figure 8 (a), the DE of semi-insulating SiC for 6 pulses is ~0.6%, whereas for 36 pulses shows a max DE of ~28% in the same semi-insulating SiC sample. The gratings are comprised of, especially with multiple pulses, a combination of amplitude

and phase causing higher DE than if they were merely phase induced. In other words, the gratings at lower energies and pulses are subsurface, which induce the phase of the phase inspection HeNe laser wavefront to be modulated. In contrast, the gratings at higher energies and pulses have surface damage that causes amplitude as well as phase modulation to the laser wavefront.

Figure 8 (b) shows how the DE varies with the grating spacing, and Figure 8 (c) represents the DE with varying grating diffraction angle of the 1st order. Figure 8 (b) and Figure 8 (c) suggests that the type of grating structure we manufactured is a volume phase grating[13]. Also, Figure 8 (b) and Figure 8 (c), show two red triangle data points which represent data added at a later date. This data was added to confirm the trends and to show repeatability in the grating fabrication. As observed, gratings added to this substrate at a later date and alignment show consistent results. Our grating structures are typically 15-35 microns deep and just below the surface resulting in a phase modulation only.

A phase modulation only grating is when only an index change, Δn, inside the bulk material has occurred, whereas, an amplitude grating is caused by surface damage/obliteration similar to a Ronchi-ruling grating (opaque lines over a transparent substrate). It is believed that for the subsurface gratings most or all DE is contributed to phase or index changes. Further measurements to confirm this will be discussed in Section 6.

The trends for the DE versus energy/fluence plot, in Figure 8(a), indicate that the efficiency *may* "roll" off or reach peak efficiency then start decreasing, but this did not happen in the semi-insulating SiC sample. Instead the DE increased quadratically even as the scattered light increased. The scattering of the light should theoretically bring the DE down, but practically the DE increased at a much higher rate than the scatter. This increase in DE is due to surface damage/charring (charring due to thermal breakdown of the chemical bonds) and to the Δn of the increased anamorphic volume. The increase in the volume depth with higher energy exposure, basically, has a longer interaction with the HeNe 632.8nm beam, used to evaluate the DE, and the gratings Δn. As mentioned, the charred surface damage decreases the DE due to scatter, but at a negligible rate as compared to the increased Δn volume. We will show later that a "roll off" did occur in conducting SiC type samples.

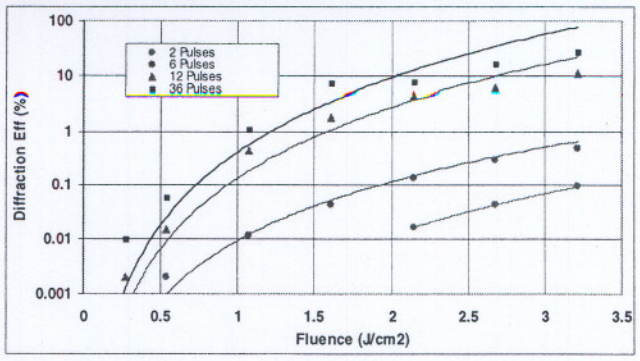

(a)

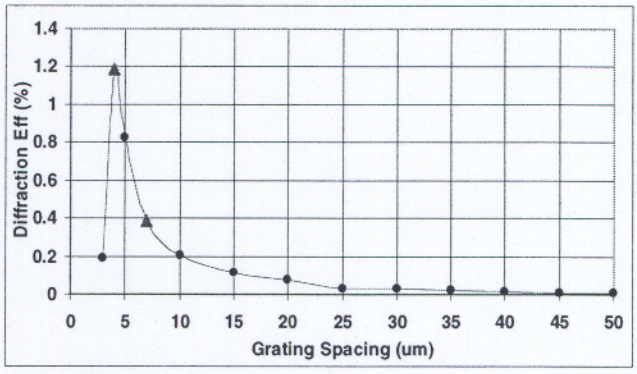

(b)

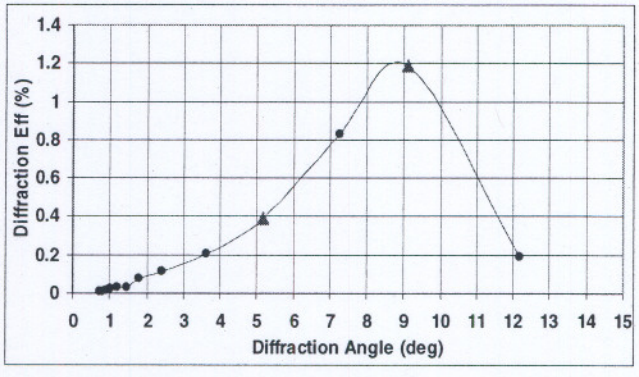

(c)

Figure 8 DE verses (a) Fluence for 2, 6, 12, and 36 pulses, (b) grating spacing and (c) diffraction angle.

5.3. SiC Conducting Grating Data/Results

Next, we tested conducting samples for comparison with the semi-insulating samples. The conducting SiC sample had a very different reaction to the laser processing, in that, the DE verses fluence started to "roll off" as the fluence increased due to absorption and scattering from the surface damage – see Figure 9. Once the DT was reached on the conducting SiC sample (for 36 pulses) there was a very discrete threshold from no damage to extreme surface thermal breakdown (or charring) – see Figure 10. At a slightly higher fluence level above the DT, the surface modifications were sporadic; leaving a discontinuous grating line with further increases would then seriously and

continuously create a solid surface modification that was black and/or opaque in color. This type of change is not desired, but we were not able to find the proper fluence level to allow for only an index modification.

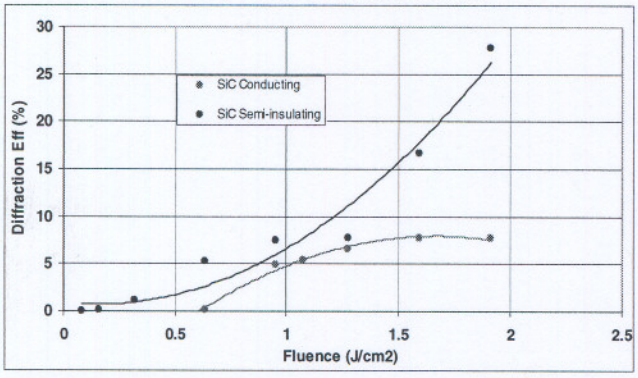

Figure 9 DE verses Fluence using 36 pulses comparing semi-insulating to conducting SiC.

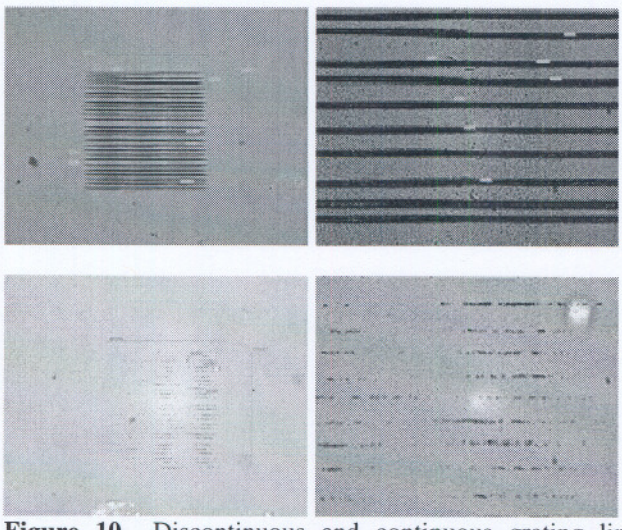

Figure 10 Discontinuous and continuous grating lines micro-machined in conducting SiC. Top two pictures, grating made using 36 pulses, and the bottom two pictures, grating made using a single pulse.

From Figure 9 and Figure 10 it is evident that the conducting SiC sample is more sensitive to the femtosecond radiation. The conducting sample has more thermal breakdown on the surface and is very sporadic for the single pulse gratings (bottom two pictures in Figure 10). Also, Figure 9 depicts this graphically by the "roll off" of the conducting SiC with increasing fluence. Also, Figure 9 shows how DE is zero and suddenly jumps to ~ 5% in less than 0.5 J/cm^2 representing the discrete threshold as described earlier.

6. SiC Characterization

The index change, Δn, in processed and unprocessed SiC semi-insulating sample was investigated by multiple techniques to understand the morphology and chemical changes. Only the semi-insulating sample was tested since the conducting SiC is opaque due to surface structural damage (charring or thermal breakdown of the molecular lattice due to the inability for the crystal to dissipate heat, and/or oxidation and chemical reactions on the surface that give a different compound such as carbon soot). The investigating methods are given below:

1. Raman Spectroscopy
2. Near Field Scanning Optical Microscopy (NSOM)
3. Atomic Force Microscopy (AFM)

The results for each of the above experiments are given in the following subsections.

6.1. Raman Spectroscopy

Raman spectra were taken from both unprocessed and processed areas. As a baseline, the Raman data was also "calibrated" with FS Raman taken that was compared to referenced FS Raman results[14] to confirm that our Raman results for SiC are valid.

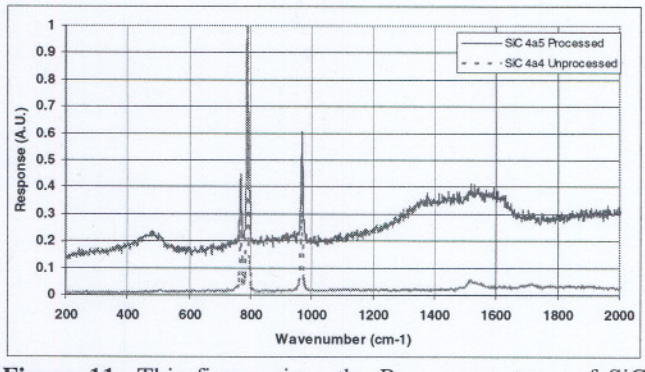

Figure 11 This figure gives the Raman spectrum of SiC semi-insulating sample of processed and unprocessed areas.

These results do show that some alterations to semi-insulating SiC have occurred. In semi-insulating SiC there is an extra spectra peak, a shift in the spectrum, and broadening. Figure 11 represents a definite change in the processed area of SiC. Table 3 gives the results in Raman spectra.

Table 3: SiC Raman spectral changes.

Type	Wavenumber (cm^{-1})
Broadening	1514
Extra Peak	480
Peak Shift	965

These affects in the Raman spectrum suggest a definite chemical change in the bond structure or that other properties have been altered by the laser processing. Multiple processed areas were tested to ensure the effect was real and repeatable. The offset from zero between the processed and unprocessed spectrums is due to an increase in background scattering.

Another test performed with Raman was focusing the Raman into the processed volume until the Raman spectrum resembled the unprocessed area as shown in Figure 11. Focusing the Raman into/through the damaged volume gave us an indication of how deep the grating lines were. This matched our previous mentioned value of 20-30μm.

6.2. *Near Field Scanning Optical Microscopy (NSOM)*

Near Field Scanning Optical Microscopy (NSOM) was completed on semi-insulating SiC in order to determine if an index change had occurred in the processed area. This test was carried out on a subsurface SiC grating to ensure no amplitude modulations were playing a role in the Δn. Figure 12 show the NSOM results.

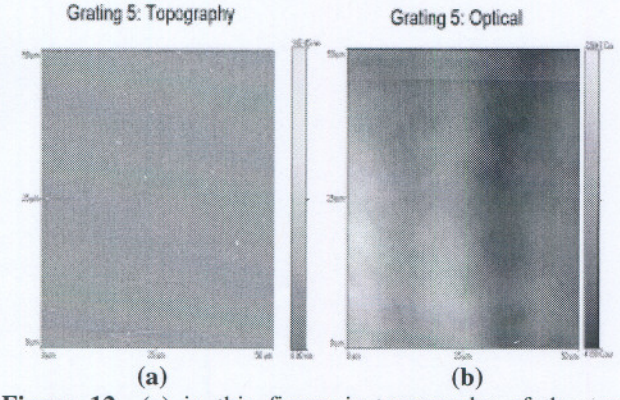

Figure 12 (a) in this figure is topography of the semi-insulating SiC sample, (b) is the optical output revealing an index change.

The NSOM optical image is generated from a collimated light source illuminating the SiC sample (~ 250μm thick) from the bottom while a fiber receiver collects the output from the top surface only, which is only ~100nm from the surface. The topography image in Figure 12 (a) shows an absence of any surface alterations due to processing, but the modifications do exist below the surface as shown in Figure 6. Figure 12 (b) demonstrates that the collimated input beam (from the bottom of the sample) is coming to a focus at the fiber receiver after propagating through the subsurface SiC grating line modifications. The grating lines act as micro-lenses consisting of convex radii and an index change in order to cause the collimated light to focus. The lighter areas in the optical image show where the light is coming to a focus at the fiber receiver, thus confirming the semi-insulating SiC sample contain a Δn only in the processed areas. The fact that this particular grating is subsurface also suggests that the modulation is phase and not amplitude. The conducting samples did not have NSOM performed due to the fact that processed structures are opaque from surface thermal breakdown or charring.

6.3. *Atomic Force Microscopy (AFM)*

Atomic Force Microscopy (AFM) was used in tapping mode to evaluate the topography of our surface gratings fabricated below the threshold. In addition to height images obtained from monitoring the cantilever oscillation amplitude during scanning, surface potential measurements can be obtained from monitoring the AFM cantilever response during an application of voltage, which gives us information on the electric field distribution. Tapping mode also allows phase images to be obtained from monitoring the dampening effects the surface has on the tip oscillation. These techniques will hopefully yield valuable data in understanding the physics of the Δn formation. Figure 13 and Figure 14 below shows some AFM results of a SiC (semi-insulating and conducting) sample with surface gratings.

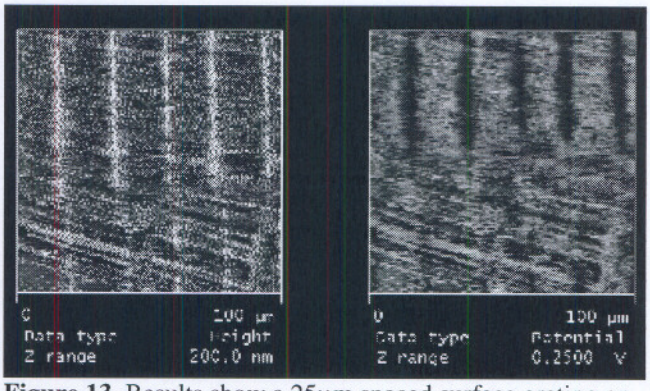

Figure 13 Results show a 25μm spaced surface grating on semi-insulating SiC material with a 0 volt surface potential applied during the AFM measurement.

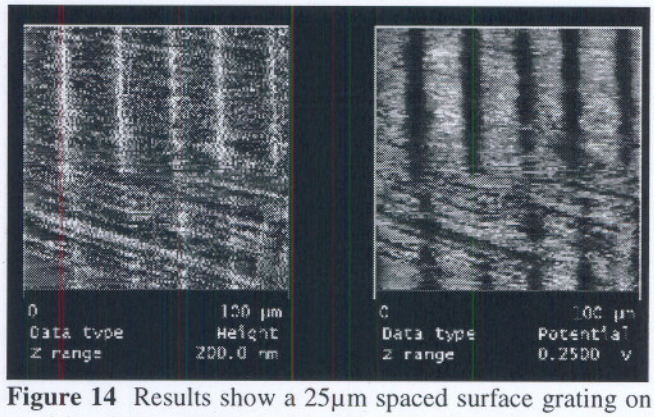

Figure 14 Results show a 25μm spaced surface grating on semi-insulating SiC material with a 5 volt surface potential applied during the AFM measurement.

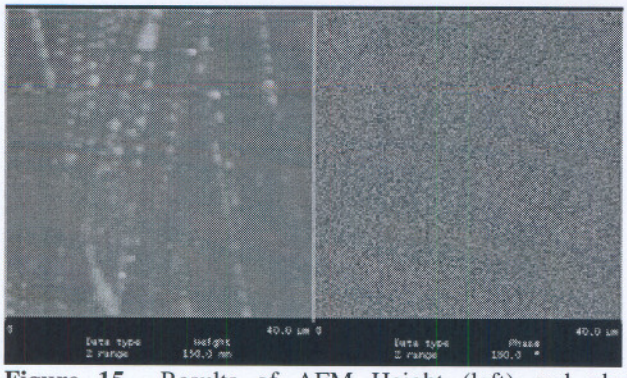

Figure 15 Results of AFM Height (left) and phase modulation (right) performed on a subsurface semi-insulating SiC grating sample.

In Figure 13 and Figure 14 represent AFM measurements on SiC semi-insulating surface grating samples. Figure 13 depicts an applied surface potential of 0 volts, while Figure 14 gives an applied surface potential of 5 volts for the same processed area. In both figures, the gratings have a 25μm period, and the AFM data concludes that the surface gratings form a hill or bulge on the surface that are roughly 20μm to 50μm in height. The surface potential images show what appears to be an increase in electric charge gathering at each processed area or grating line. No conclusive phase information of was observed. This indicates that a local subsurface restructuring has occurred or some other electronic trapping process[15] has forced the material to rise in the processed areas.

Figure 15 provides AFM data on a subsurface grating in semi-insulating SiC. Since the surface SiC gratings, shown in Figure 13 and Figure 14, confirm topological changes and show evidence for surface potential changes we decided to compare that with a subsurface grating to understand if a grating formed below the surface would retain evidence of a surface restructuring or surface potential redistribution, and if so, do these surface alterations produce HeNe laser wavefront variations (causing the beam to diffract). The AFM data taken on the subsurface grating shown in Figure 15 show that no surface modification or phase modulation exist. Further AFM images taken show no signs of surface potential variations, therefore, the HeNe laser wavefront is only being modulated from the subsurface Δn volumes (subsurface volume grating).

In summary for the AFM data:

1. Topography reveals that the processed lines are hills, not valleys.
2. Surface Potential imaging shows a concentration of charge at the processed lines.
3. The subsurface grating does not contain any topology changes, surface potential, or phase modulation.

Therefore, this AFM data provides insight as to what physical changes have occurred. The hills are likely due to the subsurface processed area forcing bulk material to bulge upward, which consist of a change in the index of refraction. As for the subsurface gratings (showing no surface distortions) the lack of surface charge and phase modulations indicate that the laser wavefront is not being distorted by the surface. Only the subsurface grating, or modified index volumes, is causing the laser wavefront to be diffracted into higher orders.

7. Conclusion

There are many methods of micromachining various transparent materials, but we have developed a new method that requires only an anamorphic lens (using three off-shelf lenses) and an ultrafast laser source. This process was tested on SiC, which is typically very difficult to process due to its hardness. We have shown diffraction efficiencies, morphology, and an index change of SiC. Future analyses of these NSOM, AFM, and Raman results along with other imaging techniques will hopefully provide better understanding on the underlying physics on what causes a change in refractive index, Δn, in transparent materials.

8. References

[1] Wright-Patterson AFB (WPAFB) Air Force Research Laboratory/Materials and Manufacturing Directorate (AFRL/MLPS), WPAFB, OH 45433, 937-255-2227.

[2] "Femtosecond History of Free Carriers in the Conduction Band of a Wide-Bandgap Oxide", Petite, Daguzan, Guizard, Martin, Service de Recherche sur les Surfaces et l'Irradiation de la Matiere, Bat. 462, CE Saclay, 91191, Gif-sur-Yvette CEDEX, France.

[3] "Short-Pulse Laser Damage in Transparent Materials as a Function of Pulse Duration", Tien, Backus, Kapteyn, Murnane, Mourou, University of Michigan, Physical Review Letters, Vol. 82, Number 19.

[4] Purdue Wide Band Gap Semiconductor Device Research Program, http://www.ecn.purdue.edu/WBG/Index.html, James Copper, Purdue University College of Engineering.

[5] "Femtosecond Pulsed Laser Ablation of 3C-SiC Thin Film on Silicon", Dong, Molian, Appl. Phys. A 77, 839-846 (2003).

[6] "Elliptic Gaussian Beam Self-focusing in Nonlinear Media", Cornolti, Lucchesi, Zambon, Optics Communications, Vol 75, No. 2, Feb. 90.

[7] "Numerical Aperture Dependence of Damage and White Light Generation from Femtosecond Laser Pulses in Bulk Fused Silica", Ashcom, Schaffer, Mazur, Dept. of Physics, Harvard University; Dept. of Chemistry & Biochemistry, University of California.

[8] "Laser Electronics", Third Edition, Verdeyen, Prentice Hall, Inc. 1995.

[9] "Femtosecond Optical Breakdown in Dielectrics", Lenzner, Kruger, Sartania, Cheng, Physical Review Letters, Vol. 80, No. 18, May 1998.

[10] "Femtosecond Ultraviolet Autocorrelation Measurements Based on Two-Photon Conductivity in Fused Silica", Strelstov, Ranka, Geata, Optics Letters, Vol. 23, No. 10, May 1998.

[11] "Self-Focusing During Femtosecound Micromachining of

Silicate Glasses", Shah, Tawney, Richardson, IEEE Journal of Quantum Electronics, Vol . 40, No. 1, Jan. 2004.

[12] "Determination of the Bandgap Offsets of the 4H-SiC/6H-SiC heterojunction Using the Vanadium Donor (0/+) Level as a Reference", Evwaraye, Smith, Mitchel, Appl. Phys. Lett. Vol. 67, No. 22, Nov. 1995.

[13] "Diffraction Grating Handbook fourth edition", Christopher Palmer, Richardson Grating Laboratory, www.gratinglab.com, Rochester, NY, 2000.

[14] "Structural Changes in Fused Silica After Exposure to Focused Femtosecond Laser Pulses", Chan, Huser, Risbud, Krol, Optics Letters, Vol. 26, No. 21, Nov. 2001.

[15] "Dynamics of Femtosecond Laser Interactions with Dielectrics", Mao, Quere, Guizard, Appl. Phys. A 79, 1695-1709, 2004.